Deformation and fracture behavior of tungsten fiber-reinforced bulk metallic glass composite subjected to transverse loading

H. Zhang, L.Z. Liu, and Z.F. Zhang[a)]
Shenyang National Laboratory for Materials Science, Institute of Metal Research, Chinese Academy of Sciences, Shenyang 110016, People's Republic of China

K.Q. Qiu
School of Materials Science and Engineering, Shenyang University of Technology, 110023 Shenyang, People's Republic of China

X.F. Pan
Shenyang National Laboratory for Materials Science, Institute of Metal Research, Chinese Academy of Sciences, Shenyang 110016, People's Republic of China; and School of Materials Science and Engineering, Tianjin University, Tianjin 300072, People's Republic of China

H.F. Zhang and Z.G. Wang
Shenyang National Laboratory for Materials Science, Institute of Metal Research, Chinese Academy of Sciences, Shenyang 110016, People's Republic of China

(Received 23 August 2005; accepted 12 December 2005)

Deformation and fracture behavior of $Zr_{41.25}Ti_{13.75}Ni_{10}Cu_{12.5}Be_{22.5}$ bulk metallic glass and its composite containing transverse tungsten fibers in compression were investigated. The monolithic metallic glass and the tungsten fiber composite specimens with aspect ratios of 2 and 1 are shown to have essentially the same ultimate strength under compression. The damage processes in the bulk metallic glass composite consisted of fiber cracking, followed by initiation of shear band in the glassy matrix mainly from the impingement of the fiber crack on the fiber/matrix interface. The site of the shear band initiation in the matrix is consistent with the prediction of finite element modeling. Evidence is present that the tungsten fiber can resist the propagation of the shear band in the glassy matrix. However, the compressive strain to failure substantially decreased in the present composite compared with the composites containing longitudinal tungsten fibers. Finally, the two composite specimens fractured in a shear mode and almost all the tungsten fibers contained cracks.

I. INTRODUCTION

Bulk metallic glasses (BMGs) have been the subject of widespread research in recent years because of their exceptional mechanical properties, such as very high fracture strength, high hardness, and low Young's moduli.[1–4] In addition, fracture toughness and fatigue crack-growth behavior of some Zr-based BMGs are similar to those of ductile alloys.[5–10] Despite these ductile features, BMGs usually exhibit little or no plasticity under uniaxial tension or compression at room temperature. Deformation of these materials is highly localized in a few shear bands, and final failure occurs by the propagation of a single dominant shear band.[4,11,12] In the past decade, mechanical properties associated with shear band formation in BMGs have attracted much attention.[13–15] Under highly confined conditions, these materials exhibit ductility as a result of the formation of multiple shear bands, which accommodate deformation without catastrophic failure.[13,16–18] Large plastic strain associated with the formation of multiple shear bands has been observed in metallic glass plates subjected to bending or in the specimens with small-aspect ratio under compression from geometrical constraint on shear band propagation.[13,16–18] Nanoindentation studies have correlated the surface deformation feature of BMGs, that is, "pop-in" phenomenon or serrated flow, with the evolution of shear bands.[14,19,20] Correspondingly, deformation mechanisms in metallic glasses are recognized to be primarily associated with the initiation and propagation of shear band.

To resist the propagation of shear band in BMGs, ductile tungsten particles or fibers have been added to metallic glasses as reinforcement to synthesize BMG composites, and improved compressive plasticity has been observed in these materials.[21–23] A plastic strain of ~7% has been obtained in a BMG composite containing ~15% tungsten particles.[21] When volume fraction of tungsten particles was increased to ~50%, a total strain as high as 16% was reached in another tungsten particulate-reinforced BMG composite.[22] Tungsten fiber-reinforced

[a)]Address all correspondence to this author.
e-mail: zhfzhang@imr.ac.cn
DOI: 10.1557/JMR.2006.0169

$Zr_{41.25}Ti_{13.75}Ni_{10}Cu_{12.5}Be_{22.5}$ matrix composites have been synthesized. The tungsten fibers are tightly bonded to the matrix because a high residual compressive radial stress exists at the fiber/matrix interface.[23] Elastic-perfectly-plastic behavior and a large improvement in plasticity have been found in this composite. This increase was associated with the formation of multiple shear bands in the glassy matrix as well as with fiber buckling.[23] Although the BMG composite containing longitudinal tungsten fibers displayed significantly improved mechanical properties, investigations have not been performed on the deformation and fracture mechanisms of the BMG composite containing transverse tungsten fibers. Therefore, little is known about how the transverse fibers affect deformation behavior and whether there is certain plasticity in such composites. The primary objective of the current study was to reveal the effect of transverse tungsten fibers on the strength and plasticity of the BMG composite and, in particular, to reveal the damage processes in the tungsten fiber and the formation of shear band in the glassy matrix for providing additional information on the deformation and fracture mechanisms of the various tungsten composites.

II. EXPERIMENTAL PROCEDURE

Tungsten fiber-reinforced $Zr_{41.25}Ti_{13.75}Ni_{10}Cu_{12.5}Be_{22.5}$ BMG composite was used in the current investigation. An ingot of the matrix material was produced by induction melting a mixture of the elemental metals in an induction furnace under an argon atmosphere. The tungsten fibers with a nominal diameter of about 300 μm were placed in the sealed end of an evacuated quartz tube. The ingot was then placed in the quartz tube and melted in a resistive furnace. A positive pressure was applied to promote infiltration of the molten alloy into the reinforcement. The sample tube was then quenched in a supersaturated brine solution. Details of the casting process are described elsewhere.[24,25]

The BMG and its composite specimens with aspect ratios of 2 and 1 were cut from the cast plate by the wire electrical discharge method. The two composite specimens had the same cross-section of 3 × 3 mm, but different heights of 6 mm (denoted as specimen A) and 3 mm (denoted as specimen B). In addition, a monolithic metallic glass specimen was produced with the same dimension as specimen A. The composite specimens were metallographically polished on the two surfaces containing the fiber ends so as to reveal the deformation features of the fibers and the matrix. Figure 1 shows a transverse cross-section of the as-received $Zr_{41.25}Ti_{13.75}Ni_{10}Cu_{12.5}Be_{22.5}$/tungsten composite observed by a S360 scanning electron microscopy (SEM; Cambridge, Cambridge, UK). It can be seen that there is no debonding or cracking at the fiber/matrix interface,

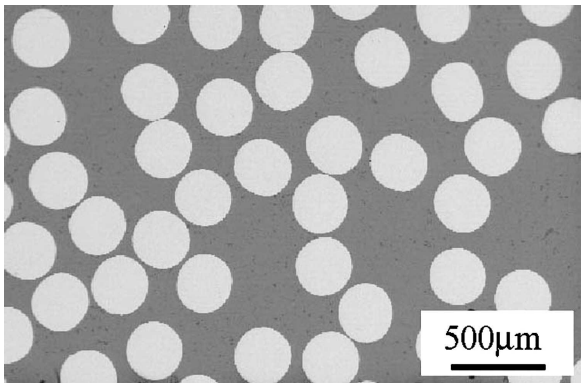

FIG. 1. SEM cross-sectional image of the as-received tungsten fiber-reinforced $Zr_{41.25}Ti_{13.75}Ni_{10}Cu_{12.5}Be_{22.5}$ metallic glass matrix composite.

and most tungsten fibers were separated by the glassy matrix. Occasionally, some fibers are closely spaced or touch each other locally. Fiber volume fractions (V_f) of the two composite specimens were measured to be ~50% by analyzing the SEM micrographs.

A compression test was performed at a strain rate of 1×10^{-4}/s using a MTS 810 material testing machine at room temperature. The tungsten fibers in the composite specimen were perpendicular to the loading axis. The composite specimens were loaded to a preselected stress level and were then unloaded to investigate their damage evolution. Microscopic observations were performed using SEM.

Compression tests were also performed on the tungsten fibers with a nominal diameter of 2 mm for comparison because the tungsten fiber with a nominal diameter of about 300 μm is difficult to handle. The longitudinal specimen had a circular cross-section and a height of ~2 mm, and the transverse specimen had a cross-section of 1.5 × 1.5 mm and a height of 1.5 mm. Both the tungsten fiber specimens were subjected to the same thermal history as those in the composites before the compression test.

To estimate the site of severe stress concentration in the composite, finite element modeling (FEM) was used to analyze elastic stress distributions in the tungsten and the glassy matrix using commercial software (ABAQUS; Abacus Concepts, Berkeley, CA). A different number of fibers is supposed to exist in the matrix, i.e., one, two, and nine fibers. In the case of two-fiber arrangement, fiber arrangements orientating along 0°, 45°, and 90° to the loading axis were considered. The nine-fiber arrangement includes triangle and square distributions. For all the fiber arrangements, the distance between two fibers is supposed to be 20 μm to induce stress concentration between two fibers. A two-dimensional plane strain model was used because of the high aspect ratio of the fiber. Choice of parameters used to calculated residual stress in the composite and details of the calculation

processes are similar to that in the literature.[26] Other elastic properties of the fiber and the matrix are listed in Tables I and II.

III. RESULTS

A. Compressive stress-strain response

Figure 2 shows the compressive stress-strain curves for $Zr_{41.25}Ti_{13.75}Ni_{10}Cu_{12.5}Be_{22.5}$ metallic glass and its composite containing transverse tungsten fibers subjected to uniaxial compression. The monolithic metallic glass fractured catastrophically without plasticity. The two composite specimens exhibited approximately the same compressive strength, but different plasticities of approximately 0.25% and 0.9%, respectively, for specimens A and B. It is apparent that the plasticity of the composite depends on the aspect ratio of the specimen: a smaller aspect ratio leads to a higher plasticity. The effect of aspect ratio on the compressive properties has also been investigated for monolithic BMGs, and the high plasticity was attributed to the mechanical constraint on the propagation of shear bands.[17,18] Because the compressive strengths of the two composite specimens and the monolithic metallic glass are nearly the same, it is believed that the compressive strength of the composite should be controlled mainly by the metallic glassy matrix.

Figure 3 shows compressive stress-strain curves for the longitudinal and transverse tungsten fiber specimens. The two specimens exhibited work-hardening during compression, and approximately the same yield strength. Additionally, the two fiber specimens can be compressed to a very high strain level (~40%), indicating a good ductility. For the tungsten fibers processed by almost the same drawing method, the strength of the 300-μm tungsten fiber was generally higher than that of the 2-mm one. Correspondingly, it is supposed that the 300-μm fiber may have nearly the same yield strength on longitudinal and transverse directions.

B. Microscopic observations of damage evolution

1. Deformation behavior of specimen A

Figure 4 shows the deformation morphologies on the side surface of the tungsten/$Zr_{41.25}Ti_{13.75}Ni_{10}Cu_{12.5}Be_{22.5}$ composite specimen A containing the fiber ends. The specimen had been loaded to a stress level of 1750 MPa, which coincides approximately with the onset of nonlinearity on the stress-strain curve in Fig. 2 (position a in Fig. 2). The deformation before failure consists of fiber cracking and shear band formation in the glassy matrix. Observations of specimen A compressed to a different strain level in Fig. 2 indicate that the first damage in the composite is the initiation of microcracks in the fibers, followed by the formation of shear bands in the glassy matrix. The microcracks in the fibers tended to initiate preferentially at certain pairs of fibers, as can be seen in Fig. 4(a). Usually, these pairs of fibers are closely spaced or even in contact with each other. Also, the angle between the line joining their centers and the loading axis is generally less than 45°. Furthermore, fibers or pairs of fibers with orientation normal to the loading axis were seldom observed to crack. In some pairs of fibers, multiple cracks were found and tended to terminate at the fiber/matrix interfaces [Fig. 4(b)], indicating a strong effect of the glassy matrix on blocking the propagation of the fiber cracks. In some regions between two closely spaced fibers, damage could only be observed in the fibers [Fig. 4(c)], further reflecting higher strength of the glassy matrix. Only a few of fiber cracks penetrated into the glassy matrix, stimulating the initiation of shear bands in the matrix, as shown in Fig. 4(d). It is observed that almost all the shear bands in the matrix were induced by the fiber cracks from the impinging on the fiber/matrix interfaces.

When the applied stress was increased to 1850 MPa, specimen A fractured with a low plasticity of only about 0.25%. Observations on the two side surfaces containing the fiber ends indicate that the specimen failed in a shear mode with fracture planes inclined about 41° and 44° to the loading axis, as shown in Figs. 5(a) and 5(b). The deviation of shear fracture angle form the maximum shear stress plane (45°) was also observed in monolithic metallic glasses and metallic glass composites and has been attributed to the effect of normal stress on the fracture process.[4,27] It is found that the fracture of specimen A proceeded predominantly in the glassy matrix, indicating that the tungsten fibers can retard or deflect the propagation of the primary shear band. This preferential propagation of the primary shear band in the glassy matrix could also be found on the fracture surface observations of specimen A. Only two tungsten fibers can be clearly seen, as in Fig. 5(c). Consequently, the shear fracture route of specimen A was not exactly planar as

TABLE I. Selected properties of metallic glass $Zr_{41.2}Ti_{13.8}Cu_{12.5}Ni_{10}Be_{22.5}$ and the tungsten composite specimen A and B.

Property	$Zr_{41.2}Ti_{13.8}Cu_{12.5}Ni_{10}Be_{22.5}$	Specimen A	Specimen B
Young's modulus (GPa)	98	125	133
Poisson's ratio	0.36		
Yield strength (MPa)	1800	1820	1830

TABLE II. Selected properties of the tungsten fibers with fiber diameters of 300 μm and 2 mm.

Property	Tungsten fiber (d = 300 μm) (longitudinal)	Tungsten fiber (d = 2 mm) (longitudinal)	Tungsten fiber (d = 2 mm) (transverse)
Young's modulus (GPa)	405	405	405
Poisson's ratio	0.28	0.28	0.28
Yield strength (MPa)	1900 (tension)	1430 (compression)	1380 (compression)

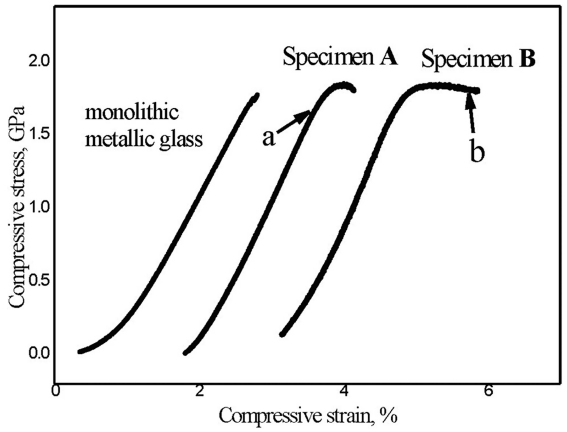

FIG. 2. Compressive stress-strain curves for $Zr_{41.25}Ti_{13.75}Ni_{10}Cu_{12.5}Be_{22.5}$ metallic glass and tungsten fiber-reinforced $Zr_{41.25}Ti_{13.75}Ni_{10}Cu_{12.5}Be_{22.5}$ metallic glass specimen A (aspect ratio 2:1) and specimen B (aspect ratio 1:1).

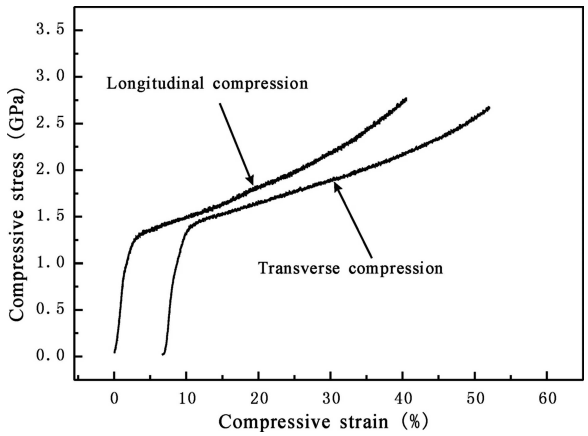

FIG. 3. Compressive stress-strain curves of the tungsten fibers oriented at different directions to the loading axis.

that of monolithic metallic glass.[4,17] Apart from the primary shear band leading to the final fracture of the specimen, there were cracks in some closely spaced tungsten fibers (four to five fibers) to connect with each other, forming two relatively long localized cracks, as indicated by the two sets of arrows in Fig. 5(a). Consequently, the fracture of specimen A may be a competitive process between primary shear band propagating through the matrix and localized cracks connecting fractured tungsten fibers. Observations on the side surfaces also indicate that only a limited quantity of shear bands formed in the glassy matrix [Fig. 5(d)], which is consistent with its poor plasticity on the stress-strain curve. Moreover, most of the shear bands are associated with fiber cracking from severe stress concentration, as shown in Fig. 5(d). These shear bands tend to initiate in the area between 0° and 45° position near the fiber/matrix interface, as indicated by the bigger arrows in Fig. 5(d). Shear band initiated at the 90° position was seldom observed, although there exists fiber cracking, as indicated by the smaller arrows in Fig. 5(d).

2. Deformation behavior of specimen B

Unlike specimen A, specimen B exhibited a delayed fracture with the characteristic of an elastic-perfectly-plastic solid. Its compressive strength is almost the same as that of specimen A (Fig. 2). Figure 6(a) shows the deformation morphology of specimen B after having been loaded into the plateau region of its stress-strain curve (corresponding to point b in Fig. 2 and a total strain of about 2.7%). Two primary cracks were formed by connecting severely cracked fibers and shear bands in the matrix, as indicated by the two sets of arrows in Fig. 6(a). The two primary cracks traversed almost the entire cross-section of the specimen at this strain level without leading to a sudden fracture of the specimen [Fig. 6(b)]. Compared with specimen A, more fine and short shear bands were found to form in the glassy matrix, and most of them appear to be associated with the stress concentration at the fiber/matrix interfaces, as shown in Fig. 6(c). These shear bands tended to initiate preferentially in the region between two closely spaced fibers, as indicated by the bigger arrows in Fig. 6(c). Moreover, the area between 0° and 45° near the fiber/matrix interface was also the preferential site for shear band initiation, as indicated by the small arrows in Fig. 6(c). Shear bands initiated at the 90° position were seldom observed, consistent with the observation in specimen A. However, most shear bands propagated only across the regions between any two fibers before being blocked by the neighboring fibers, and the tungsten fibers could not be cut through easily [Fig. 6(d)]. It is apparent that the tungsten fiber plays a role in blocking the propagation of shear band. Along the two primary cracks, coarser shear bands can be observed and are usually associated with the severely damaged fibers. Final failure of specimen B occurred along the two primary cracks by the linking of severely cracked fibers and the coarse shear bands in the matrix.

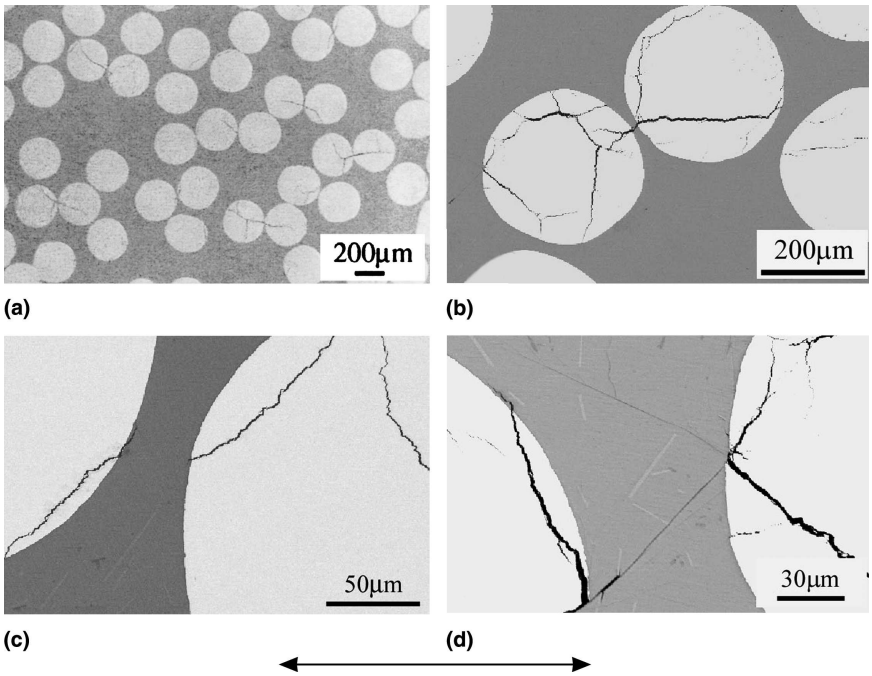

FIG. 4. SEM of specimen A, unloaded from a stress level of 1700 MPa. (a) Microcracks exclusively nucleated in some pairs of tungsten fibers, (b) multiple cracks in a tungsten fiber, (c) cracks preferentially formed in the tungsten fibers, and (d) shear bands in the matrix, which initiated at the fiber/matrix interface because of impingement of the cracks in the fiber on the interface. The arrow on the bottom indicates direction of loading axis.

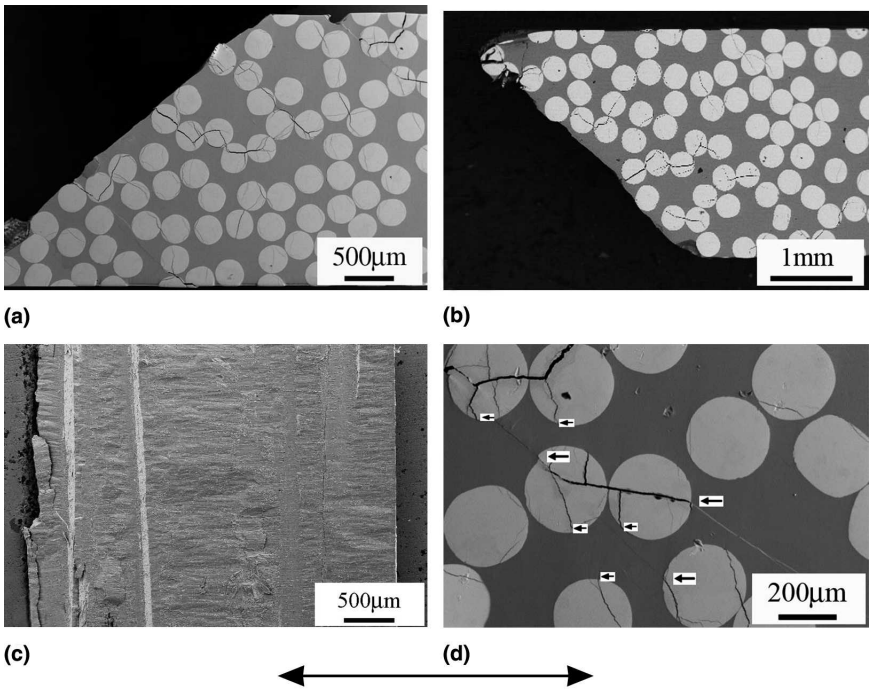

FIG. 5. SEM of specimen A after fracture. (a) Shear fracture at an angle of ~41° observed on one surface. Two localized cracks connecting a few cracked fibers (see arrows) were also formed when the composite fractured, (b) shear fracture at an angle of ~44° observed on the other side surface, (c) low magnification of the fracture surface containing two fibers, and (d) only a few shear bands formed in the glassy matrix. The arrow on the bottom indicates direction of loading axis.

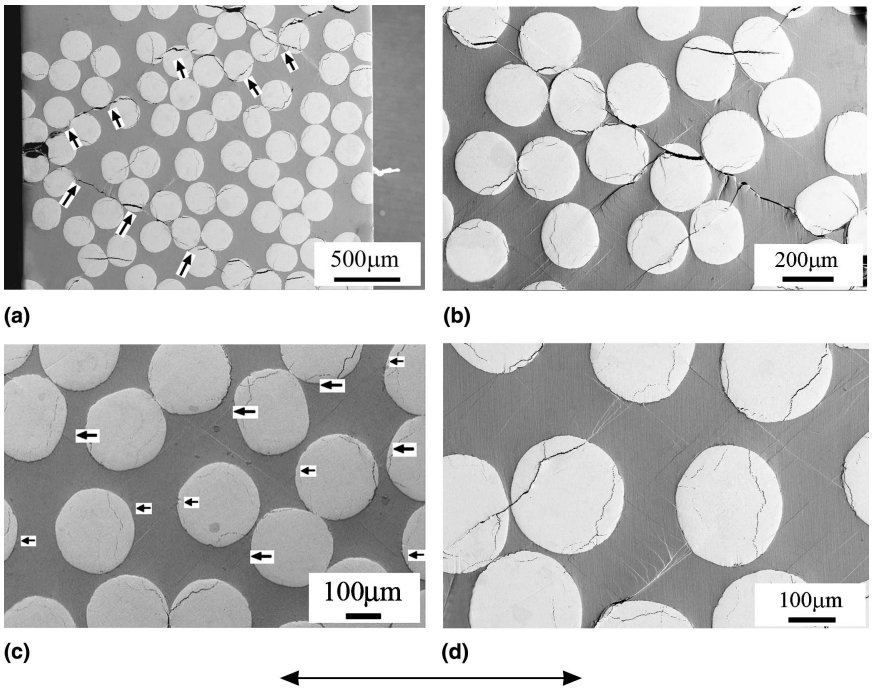

FIG. 6. Deformation morphologies of specimen B, unloaded from a total strain of 2.7%, which corresponds to the position b in Fig. 2. (a) Two primary cracks (indicated by arrows) connecting cracked fibers and shear bands in the matrix (note that some shear bands have developed into cracks), (b) multiple shear bands in the matrix, (c) shear bands induced by stress concentration at the fiber and fiber/matrix interfaces, and (d) propagation of coarse shear bands blocked by tungsten fibers. The arrow on the bottom indicates direction of loading axis.

IV. DISCUSSION

In contrast to the obvious increase in compressive strain observed in tungsten composites containing longitudinal fibers,[23] the transverse fiber composite specimen studied here failed with little plasticity, although both of them have an approximately the same fiber volume fraction of about 50%. Moreover, the compressive strength, the plasticity, and fracture mode of specimen A are similar to those of its unreinforced counterpart. The plasticity of the composite specimen with a low aspect ratio is strongly affected by the transverse tungsten fibers. Therefore, different mechanisms will be discussed concerning damage of fibers, shear bands in the glassy matrix, and the interaction between the fiber and the matrix.

A. Fiber cracking

One of the interesting findings in the deformed composite containing transverse fibers is that fiber cracking occurred before the formation of shear band in the matrix, and microcracks initiated preferentially at some closely spaced tungsten fibers. Before compression, the fibers were in a state of residual compression and were highly constrained by the glassy matrix because of the difference in thermal expansion coefficient between the fiber and the matrix.[23] Dragoi et al.[26] have calculated the residual stress in a tungsten fiber/$Zr_{41.25}Ti_{13.75}Ni_{10}Cu_{12.5}Be_{22.5}$ composite using FEM and found that a severe stress concentration existed in the regions between those closely spaced fibers. Elastic FEM analysis for the distribution of the von Mises stress in the BMG composite containing transverse fibers after taking the residual stress into account is shown in Fig. 7. The analysis combines the residual thermal stress and a uniaxial compressive stress of 1800 MPa. It can be seen from all the cases of fiber distribution that under the remotely applied transverse compressive load, higher stress is induced in the tungsten fibers and in the glassy matrix between two closely spaced fibers compared with regions where fibers are well spaced. Moreover, for the two-fiber arrangement, the stresses in the two fibers are always higher than that in the glassy matrix between the two fibers. Localized stress in these tungsten fibers may have surpassed the transverse fracture strength of the tungsten fiber, leading to preferential crack initiation in these tungsten fibers, consistent with the observation in Fig. 4(a). On the other hand, the high stress in the matrix between two closely spaced tungsten fibers could also have been relaxed through generation of cracks in the neighboring two fibers, leading to delayed initiation of shear band in the glassy matrix.

B. Shear bands in the glassy matrix

In general, the plastic deformation of metallic glasses is essentially confined in narrow regions near the shear bands. This implies that the extent of plastic deformation of metallic glasses depends on the total number of shear

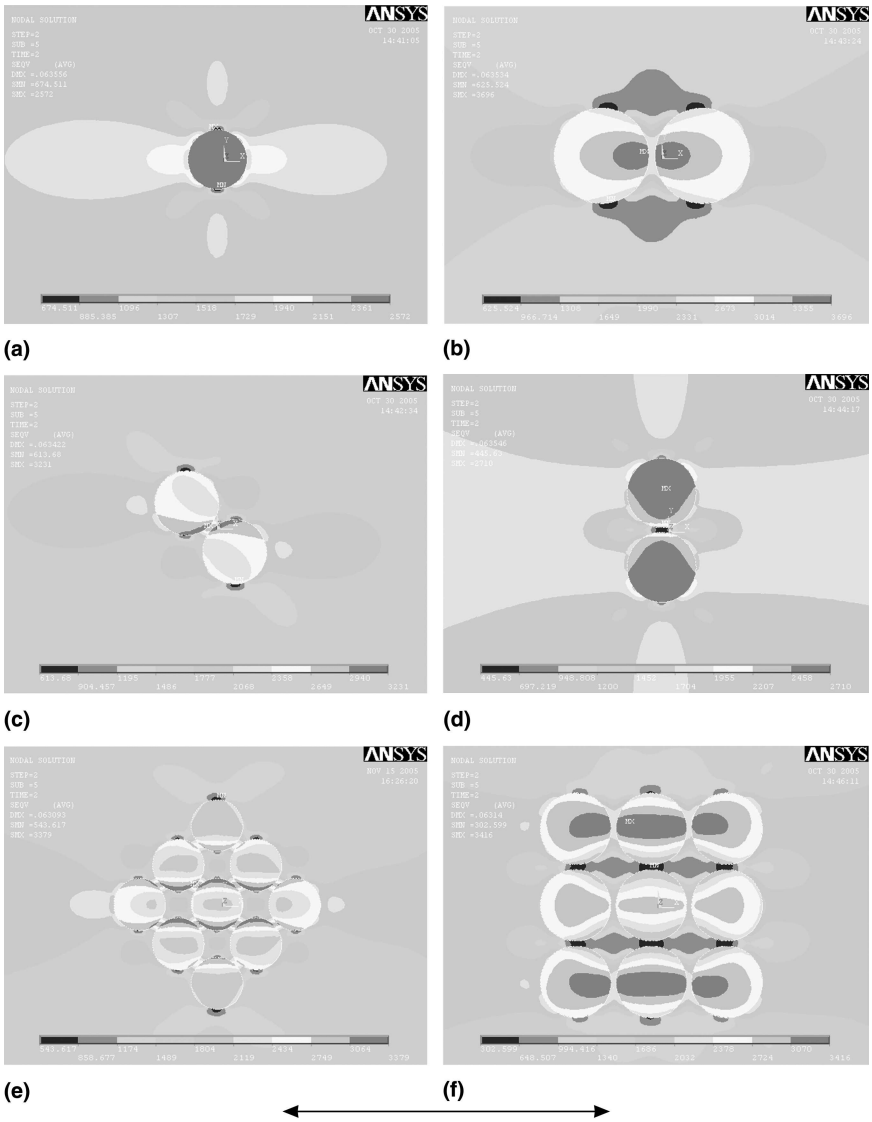

FIG. 7. FEM analysis result of von Mises stresses in the 50% V_f tungsten fiber-reinforced BMG composite with different tungsten fiber amounts and arrangements. (a) One fiber, (b) two fibers at 0° direction, (c) two fibers at 45° direction, (d) two fibers at 90° direction, (e) triangle array of nine fibers, and (f) square array of nine fibers. The arrow on the bottom indicates direction of loading axis.

bands in the specimen and the shear step height of a shear band on the specimen surface.[28–30] In contrast to the strong toughening effect observed in the BMG composites with about 50% volume fraction of particles or fibers,[22,23] very limited plastic deformation was observed in the present composite specimens even though the fiber volume fraction of the tungsten fiber is also as high as 50%. This should be associated with the limited number of shear bands across the whole specimen or with the small slip displacement in the shear bands between the tungsten fibers[28] [Figs. 5(d) and 6(b)].

Specimen A fractured as a result of propagation of a primary shear band along 41° or 44° directions on the either sides of the specimen [Figs. 5(a) and 5(b)]. Additionally, the primary shear bands tend to propagate in the region with sparse fiber distribution. The tungsten fiber can effectively block the propagation of the shear bands in the matrix. Consequently, for plasticity improvement consideration, it is important to focus attention on optimizing fiber arrangement to retard or block the propagation of the shear bands in the glassy matrix. Two uniformly distributed fiber arrangements, e.g., a square and a triangular array of fibers are suggested for a 50% V_f fiber composite, as schematically illustrated in Fig. 8. From the present experimental results and the possible shear fracture angles of the tungsten composite observed in Figs. 5(a) and 5(b), three possible shear fracture planes of 41°, 45°, and 49° are considered in Fig. 8. It is apparent that the square array of fiber arrangement may provide the lowest resistance to the propagation of shear band

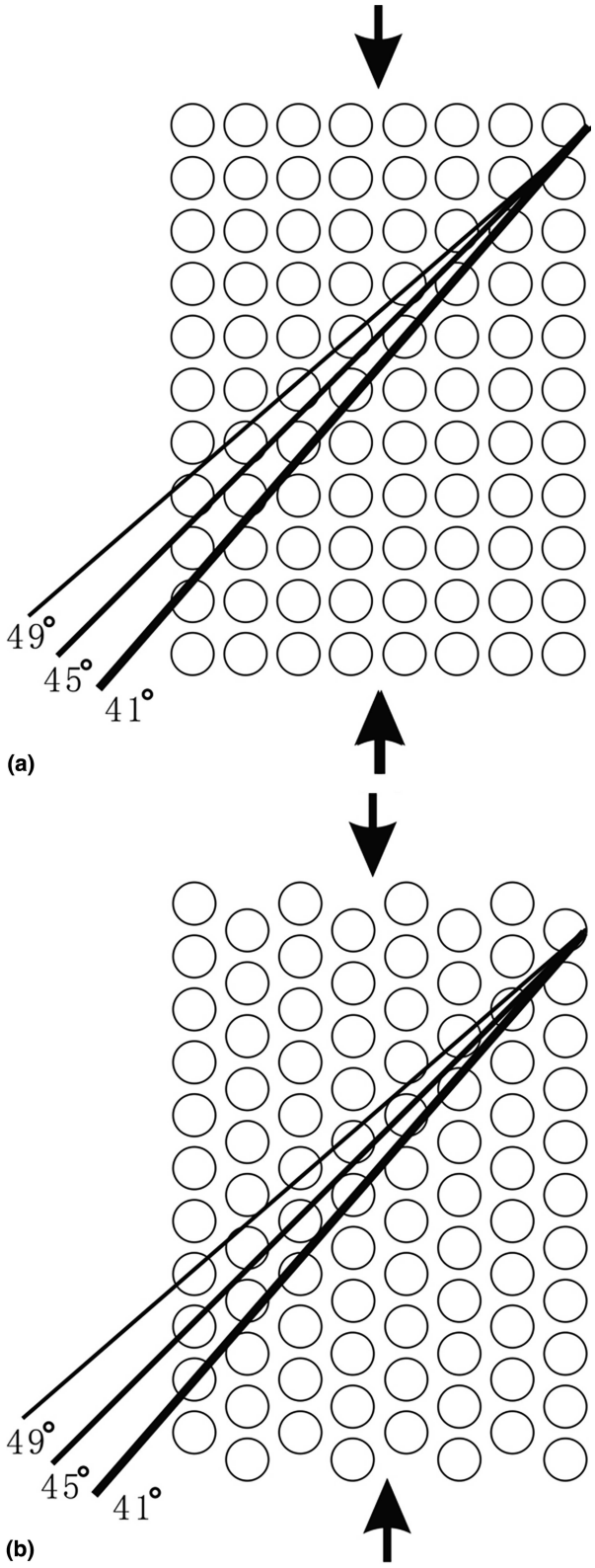

FIG. 8. Schematic illustration of two different fiber arrangements and three different shear planes with different angles with respect to the loading axis in a 50% V_f tungsten fiber composite. (a) Square array of fiber arrangement and (b) triangle array of fiber arrangement. Note that the lowest resistance is on the 45° shear plane for the square array of fiber arrangement.

along the 45° shear plane. Consequently, the uniform and triangular array of fibers may be superior to the square array in blocking the propagation of shear bands under compression.

Specimen A fractured in a shear mode with shear fracture angle of 41° or 44°, indicating that the angle between shear fracture plane and the loading axis is smaller than 45°. This deviation from the maximum shear stress plane was also observed in monolithic BMGs and their composites.[4,15,27,31] Mohr–Coulomb criterion is considered for this deviation by taking the effect of the normal stress into account,[4,27] i.e.,

$$\tau_\theta - \mu\sigma_\theta \geqslant \tau_0 \quad ,$$

where μ is a material constant, σ_θ and τ_θ are the normal and shear stresses on any shear plane, and τ_o is the critical shear fracture stress without normal stress. In addition to the primary shear band that caused the shear fracture of specimen A, two localized cracks connecting cracked fibers also formed before fracture [Fig. 5(a)]. These localized cracks are oriented parallel to or slightly tilted from the loading axis, and may eventually have caused longitudinal splitting of the composite. This competitive process between shear fracture and longitudinal splitting is, to some extent, similar to the tungsten composites, with fibers aligned parallel to the loading axis.[23,32] For these composites, it is the failure mode changed from shear fracture to longitudinal splitting when the fiber volume fraction was increased.[23,32] Supposing the tungsten fibers are uniformly distributed in the glassy matrix, specimen A would still fail in a shear mode instead of by longitudinal splitting because shear bands in the matrix normally propagated at about 45° to the loading axis. The final failure of the specimen may occur by connecting cracked fibers and shear bands in the matrix. Localized cracks [similar to that in Fig. 5(a)] will no longer form because of the uniform arrangement of the tungsten fibers.

C. Interactions between the tungsten fiber and the shear band

For monolithic metallic glassy specimen with low aspect ratios, multiple shear bands were frequently observed to initiate from the upper and bottom edges of the specimen and then propagate toward the center of the specimen.[18] For specimen B, many shear bands were observed to form in the glassy matrix between the tungsten fibers [Figs. 6(c) and 6(d)], not to be related to the edge effect of the specimen. This demonstrates that the tungsten fibers may have stimulated the initiation or block the propagation of shear bands in the matrix. Difference in the elastic modulus between the matrix and the tungsten fibers is expected to cause a large difference in the elastic stress upon loading of the composite, which

would have caused stress concentration at the fiber/matrix interfaces, promoting shear band initiation in the matrix [Figs. 5(d) and 6(c)]. Observations in the deformed glassy matrix demonstrate that the shear bands in the matrix usually initiate in the area between two closely spaced fibers or near the fiber/matrix interfacial region between 0° and 45° position. This is consistent with the FEM result, which predicted that severe stress concentration existed in the area where fibers are closest to each other. Additionally, severe stress concentration tended to occur in the area between 0° and 45° position near fiber/matrix interface (Fig. 7). Because of the high stress concentration, the shear bands would have developed into cracks and connect with the cracked fibers, causing the final fracture of the composite. Consequently, substantially decreased plasticity was observed for specimen B compared with its monolithic glass counterpart.[18]

In metallic glass composites, multiple shear bands usually formed as a result of constraint effect of the reinforcement on shear band propagation.[23,28] Similarly, the propagation of the shear bands in the matrix was usually blocked by the tungsten fibers, leading to the formation of secondary shear bands parallel to the primary one [Fig. 6(d)]. The strong blocking effect of the tungsten fiber is also evidenced by the fact that the fibers could not be easily cut through even though the coarse shear bands had developed into cracks. Final failure of the composites had to occur by linking the cracks in the fibers and nearly paralleled shear bands in the glassy matrix.

V. CONCLUSIONS

In this article, we conclude that: (i) the BMG composite specimens containing transverse tungsten fibers exhibited approximately the same compressive strength and shear fracture angle as those in $Zr_{41.25}Ti_{13.75}Ni_{10}Cu_{12.5}Be_{22.5}$ metallic glass, indicating that the mechanical properties of the BMG composites are mainly dominated by the glassy matrix. (ii) The addition of transverse tungsten fibers to metallic glass may not substantially increase the plasticity of the composite specimen with a low aspect ratio compared with its unreinforced counterpart. This can be attributed to the formation of primary cracks connecting cracked fibers and shear bands or cracks in the glassy matrix in the early stages of plastic deformation. (iii) The fiber cracking or fiber/matrix interface can effectively stimulate the formation of shear bands in the glassy matrix from stress concentration. (iv) The orientation of those shear bands tends to occur in the area between 0° and 45° position near the fiber/matrix interface, consistent with the sites of severe stress concentration predicted by FEM analysis. Some of the shear bands in the glassy matrix may develop into cracks because of the impingement of the fiber cracking on the fiber/matrix interface. However, the tungsten fibers could not be cut through by the shear bands or the propagating cracks, providing strong resistance to the propagation of shear bands.

ACKNOWLEDGMENTS

We thank G. Yao, J.L. Wen, H.H. Su, and W. Gao for technical assistance and stimulating discussions. This work was supported by the National Natural Science Funds of China under Grant Nos. 50401019 and 50323009 and by the Chinese Academy of Sciences "Hundred of Talents Project."

REFERENCES

1. A. Inoue: Stabilization of metallic supercooled liquid and bulk amorphous alloys. *Acta Mater.* **48,** 279 (2000).
2. W.L. Johnson: Bulk glass-forming metallic alloys: science and technology. *MRS Bull.* **24,** 42 (1999).
3. J.F. Löffler: Bulk metallic glasses. *Intermetallics* **11,** 529 (2003).
4. Z.F. Zhang, G. He, J. Eckert, and L. Schultz: Fracture mechanisms in bulk metallic glassy materials. *Phys. Rev. Lett.* **91,** 045505 (2003).
5. P. Lowhaphandu and J.J. Lewandowski: Fracture toughness and notched toughness of bulk amorphous alloy: Zr-Ti-Ni-Cu-Be. *Scripta Mater.* **38,** 1811 (1998).
6. K.M. Flores and R.H. Dauskardt: Local heating associated with crack tip plasticity in Zr-Ti-Ni-Cu-Be bulk amorphous metals. *J. Mater. Res.* **14,** 638 (1999).
7. P. Lowhaphandu, L.A. Ludrosky, S.L. Montgomery, and J.J. Lewandowski: Deformation and fracture toughness of a bulk amorphous Zr–Ti–Ni–Cu–Be alloy. *Intermetallics* **8,** 487 (2000).
8. P.A. Hess and R.H. Dauskardt: Mechanisms of elevated temperature fatigue crack growth in Zr–Ti–Cu–Ni–Be bulk metallic glass. *Acta Mater.* **52,** 3525 (2004).
9. C.J. Gilbert, V. Schroeder, and R.O. Ritchie: Mechanisms for fracture and fatigue-crack propagation in a bulk metallic glass. *Metall. Mater. Trans. A* **30,** 1739 (1999).
10. H. Zhang, Z.G. Wang, K.Q. Qiu, Q.S. Zang, and H.F. Zhang: Cyclic deformation and fatigue-crack propagation of a Zr-based bulk amorphous metal. *Mater. Sci. Eng.* **A356,** 173 (2003).
11. T.G. Nieh, C. Schuh, J. Wadsworth, and Y. Li: Strain rate-dependent deformation in bulk metallic glasses. *Intermetallics.* **10,** 1177 (2002).
12. J. Eckert, A. Reger-Leonhard, B. Weiss, and M. Heilmaier: Nanostructured materials in multicomponent alloy systems. *Mater. Sci. Eng.* **301,** 1 (2001).
13. G. Ravichandran and A. Molinari: Analysis of shear banding in metallic glasses under bending. *Acta Mater.* **53,** 4087 (2005).
14. C.A. Schuh and T.G. Nieh: A nanoindentation study of serrated flow in bulk metallic glasses. *Acta Mater.* **51,** 87 (2003).
15. Z.F. Zhang, G. He, and J. Eckert: Shear and distensile fracture behaviour of Ti-based composites with ductile dendrites. *Philos. Mag.* **85,** 897 (2005).
16. R.D. Conner, Y. Li, W.D. Nix, and W.L. Johnson: Shear band spacing under bending of Zr-based metallic glass plates. *Acta Mater.* **52,** 2429 (2004).
17. H.A. Bruck, T. Christman, A.J. Rosakis, and W.L. Johnson: Quasi-static constitutive behavior of $Zr_{41.25}Ti_{13.75}Ni_{10}Cu_{12.5}Be_{22.5}$ bulk amorphous alloys. *Scripta Metall. Mater.* **30,** 429 (1994).
18. Z.F. Zhang, H. Zhang, X.F. Pan, J. Das, and J. Eckert: Effect of

aspect ratio on the compressive deformation and fracture behavior of Zr-based metallic glass. *Philos. Mag. Lett.* **85,** 513 (2005).

19. R. Vaidyanathan, M. Dao, G. Ravichandran, and S. Surash: Study of mechanical deformation in bulk metallic glass through instrumented indentation. *Acta Mater.* **49,** 3781 (2001).
20. A.L. Greer, A. Castellero, S.V. Madge, I.T. Walker, and J.R. Wilde: Nanoindentation studies of shear banding in fully amorphous and partially devitrified metallic alloys. *Mater. Sci. Eng.* **A375,** 1182 (2004).
21. R.D. Conner, H. Choi-Yim, and W.L. Johnson: Mechanical properties of $Zr_{57}Nb_5Al_{10}Cu_{15.4}Ni_{12.6}$ metallic glass matrix particulate composites. *J. Mater. Res.* **14,** 3292 (1999).
22. H. Choi-Yim, J. Schroers, and W.L. Johnson: Microstructures and mechanical properties of tungsten wire/particle reinforced $Zr_{57}Nb_5Al_{10}Cu_{15.4}Ni_{12.6}$ metallic glass matrix composites. *Appl. Phys. Lett.* **80,** 1906 (2002).
23. R.D. Conner, R.B. Dandliker, and W.L. Johnson: Mechanical properties of tungsten and steel fiber reinforced $Zr_{41.25}Ti_{13.75}Cu_{12.5}Ni_{10}Be_{22.5}$ metallic glass matrix composites. *Acta Mater.* **46,** 6089 (1998).
24. K.Q. Qiu, A.M. Wang, H.F. Zhang, B.Z. Ding, and Z.Q. Hu: Mechanical properties of tungsten fiber reinforced ZrAlNiCuSi metallic glass matrix composite. *Intermetallics* **10,** 1283 (2002).
25. R.B. Dandliker, R.D. Conner, and W.L. Johnson: Melt infiltration casting of bulk metallic-glass matrix composites. *J. Mater. Res.* **13,** 2896 (1998).
26. D. Dragoi, E. Ustundag, B. Clausen, and M.A.M. Bourke: Investigation of thermal residual stresses in tungsten-fiber/bulk metallic glass matrix composites. *Scripta Mater.* **45,** 245 (2001).
27. Z.F. Zhang, J. Eckert, and L. Schultz: Difference in compressive and tensile fracture mechanisms of $Zr_{59}Cu_{20}Al_{10}Ni_8Ti_3$ bulk metallic glass. *Acta Mater.* **51,** 1167 (2003).
28. H. Choi-Yim, R. Buschi, U. Köster, and W.L. Johnson: Synthesis and characterization of particulate reinforced $Zr_{57}Nb_5Al_{10}Cu_{15.4}Ni_{12.6}$ bulk metallic glass composites. *Acta Mater.* **47,** 2455 (1999).
29. J.C. Lee, Y.C. Kim, J.P. Ahn, and H.S. Kim: Enhanced plasticity in a bulk amorphous matrix composite: Macroscopic and microscopic viewpoint studies. *Acta Mater.* **53,** 129 (2005).
30. B. Moser, J. Kuebler, H. Meinhard, W. Muster, and J. Michler: Observation of instabilities during plastic deformation by in-situ SEM indentation experiments. *Adv. Eng. Mater.* **7,** 388 (2005).
31. W.J. Wright, R. Saha, and W.D. Nix: Deformation mechanisms of the $Zr_{40}Ti_{14}Ni_{10}Cu_{12}Be_{24}$ bulk metallic glass. *Mater. Trans.* **42,** 642 (2001).
32. H. Zhang, Z.F. Zhang, Z.G. Wang, K.Q. Qiu, H.F. Zhang, and Q.S. Zang: Effects of tungsten fibers on fracture modes of Zr-based bulk metallic glassy composites. *Metall. Mater. Trans. A* (2005, in press).